

A Mobility Model Correction for ‘Atomistic’ Drift-Diffusion Simulation

S. M. Amoroso[‡], C. L. Alexander^{*}, S. Markov^{*}, G. Roy[†], and A. Asenov^{**†}

^{*}Dipartimento di Elettronica e Informazione, Politecnico di Milano-IU.NET, Milano, Italy

^{*}Device Modelling Group, School of Engineering, University of Glasgow, Glasgow, G12 8LT, UK

[†]Gold Standard Simulations Ltd, Rankine Building, Oakfield Avenue, Glasgow, G12 8LT, UK

amoroso@elet.polimi.it

Abstract – A comprehensive statistical investigation of the increase in resistance associated with charge trapping in ‘atomistic’ simulations is presented considering a wide range of doping densities and mesh spacing for both classical and quantum formalisms. A modified mobility model for the ‘atomistic’ simulations is proposed to suppress the error related to the fictitious charge trapping.

Keywords–Atomistic Simulation, Mobility Model, Density Gradient

I. INTRODUCTION

Resolving individual charges within classical Drift Diffusion [1] using a fine mesh is problematic [2-3]. Due to the use of Boltzmann or Fermi-Dirac statistics in numerical simulation the electron concentration follows the electrostatic potential, obtained from the solution of the Poisson equation. As a result a significant amount of mobile charge can become trapped in sharply resolved Coulomb potential wells created by discrete dopant charges. Such trapping is not physical as, in quantum mechanical terms, confinement keeps the ground electron state high in the well. Additionally the quantity of trapped charge is strongly sensitive to the mesh size in classical drift-diffusion simulations [4]. One possible solution is to use a quantum mechanically consistent treatment of the electron concentration via the Density Gradient (DG) approximation [4]. A previous simulation study of a highly doped ($N_D=10^{20} \text{ cm}^{-3}$) resistor [4] has shown that the DG approach removes the mesh-dependent resistance problem, but a residual not negligible error remains in the evaluation of the average ‘atomistic’ resistance when compared to the calculated analytical value.

In this work we present a comprehensive statistical investigation of the increase in resistance associated with charge trapping in ‘atomistic’ simulations, considering a wide range of doping densities ($N_D=10^{17}-10^{21} \text{ cm}^{-3}$) and mesh spacing (0.5-2nm) for both classical and DG formalisms.

II. SIMULATION METHODOLOGY

In order to study the charge trapping phenomena associated with ‘atomistic’ simulation, a silicon resistor with n-type doping and dimensions $50 \times 50 \times 50 \text{ nm}$ was chosen as test structure and an ensemble of a thousand microscopically different devices were simulated for each doping density and each mesh spacing using the GSS[†] ‘atomistic’ simulator GARAND. A Cloud-in-Cell (CIC) [5] method is adopted for the charge assignment in the simulations. The continuously doped case is taken as the reference as it matches the

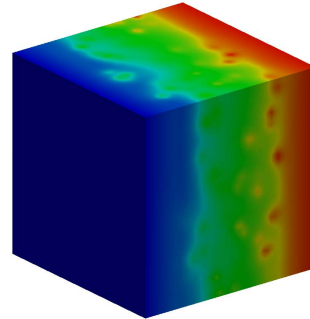


Figure 1. 3D plot of the effective potential in a $50 \times 50 \times 50 \text{ nm}$ silicon resistor doped at $1 \times 10^{19} \text{ cm}^{-3}$. Note that the region with the discrete doping is long 30nm.

analytical conductivity of the resistor. In section III it is demonstrated that the observed increase in resistance within ‘atomistic’ simulations represents a simulation artifact and cannot be ascribed to any physical conduction mechanism.

The electron mobility in ‘atomistic’ simulations is calculated, via the Masetti model [6], using the continuous doping profile. Hence, for each doping density, all atomistic devices use the same calculated mobility. Additionally, when specified, an electric field dependent mobility is also adopted in simulations. In this case the mobility depends on the local electric field generated by each discrete dopant. As shown in section III, this represents an additional source of error and variability for the atomistic resistance. It should be noted (Fig. 1) that the atomistic region length is 30 nm. A continuously doped region is interposed between the contacts and the discrete zone to avoid any influence related to boundary conditions.

The potential distribution for one of the simulations is shown in Fig. 1 for a doping value of $N_D=10^{19} \text{ cm}^{-3}$.

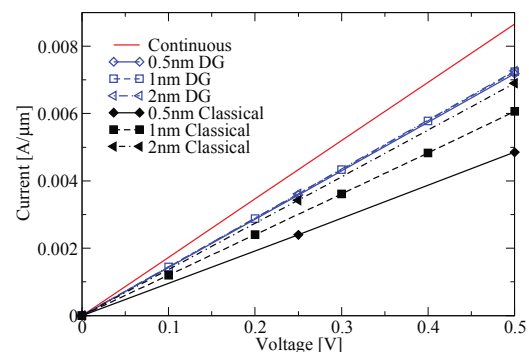


Figure 2. Comparison of the IV characteristics produced from classical and DG simulation on ensembles of 1000 atomistically different devices with mesh spacings of 0.5, 1 and 2nm.

III. RESULTS AND DISCUSSION

Fig. 2 depicts the average I-V characteristics obtained from classical and DG simulations of the resistor, for a doping value of $N_D=10^{19} \text{ cm}^{-3}$ and a mesh spacing of 0.5nm, 1 nm

and 2nm. As can be seen from Fig. 2 the resistance of the device increases dramatically in the ‘atomistic’ classical cases, showing a strong mesh dependence. DG results are mesh-independent and closer to the analytical result, but a discrepancy remains between the ‘atomistic’ average resistance and the analytical resistance. This difference is related to the electron concentration profile through the device (Fig. 3). It should be noted that the integral of charge density over the device volume is the same for both the average ‘atomistic’ resistor and the continuously doped resistor. Fig. 3 shows that the DG approach smoothes the electron density profile with respect to the classical approach, reducing the effect of charge trapping.

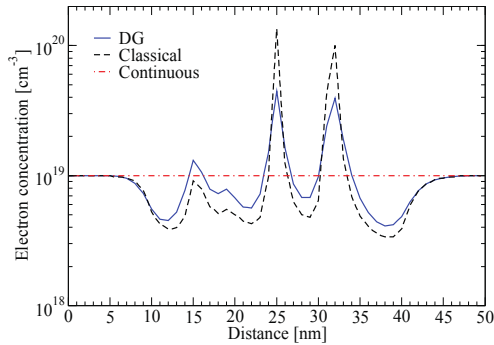


Figure 3. 1D plot of the electron concentration through a 50x50x50nm silicon resistor doped at $1 \times 10^{19} \text{ cm}^{-3}$, comparing the profile obtained from classical and DG simulations.

Fig. 4 shows the relative error between the average ‘atomistic’ resistance and the analytical resistance for different doping densities and different mesh spacing values for both classical and DG simulations. As before it can be seen that classical simulations have a larger error than DG simulations. It can also be seen that all simulations exhibit a similar shape. Starting at low doping densities the error increases until it reaches a maximum of around 10^{19} cm^{-3} and then decreases for higher doping densities.

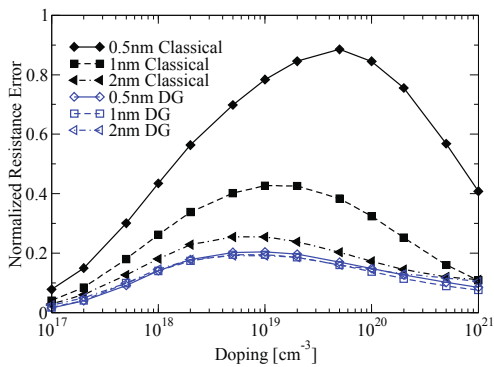


Figure 4. The relative error of the resistance calculated in a 50x50x50nm silicon resistor using both classical and DG formalisms for various mesh spacing and doping densities.

This shape can be explained if we first consider high doping densities. Fig. 5 shows that the height of the potential peaks causing electron trapping decreases when the doping concentration increases. This can be due to the reduction of the Debye length (λ_D), causing an increase in the electrostatic screening, or the reduction of the average distance between dopants

(d_{avg}), causing a smoothing of the interactive potential wells. The inset in Fig. 5 shows that λ_D decreases more quickly than d_{avg} when the doping concentration increases, suggesting that the electrostatic screening is the major factor responsible for the reduction in peak height. This is confirmed in Fig.6 where the 1D electrostatic potential along a resistor is shown when a single discrete dopant is placed at the center of the device with varying continuous background doping densities (D_{bg}).

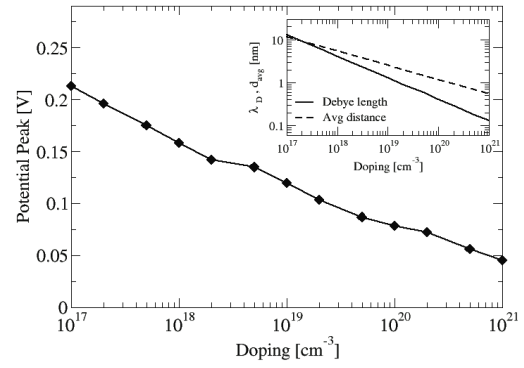


Figure 5. Potential peaks height in 3D resistor simulation as a function of the average doping density. The Inset shows the trend of the Debye length (λ_D) and of the average distance between dopants (d_{avg}) with the doping density.

Our previous analysis implies that the error in the resistance should increase as the doping density decreases. However Fig. 4 shows that the error in the resistance decreases at low doping densities. In order to understand this behavior the electron conduction profile is studied in more detail. Contrary to the situation in a MOSFET channel, the discrete dopants in a resistor are attractive potentials for electrons. As a result, the current density maxima are found corresponding to the dopants positions. This is clearly shown in Fig. 7(a) which shows a plot of the electron current density taken through the center of a resistor with a single discrete dopant placed at the center. However, if we integrate the current density inside the dashed circle (region B, representing the region where the potential peak of Fig.7(b) has the largest impact) then we obtain a current one order of magnitude smaller than the current flowing outside the dashed circle (region A). This implies that, the carrier current still follows a percolative path between the discrete dopants, when few dopants are present in the device.

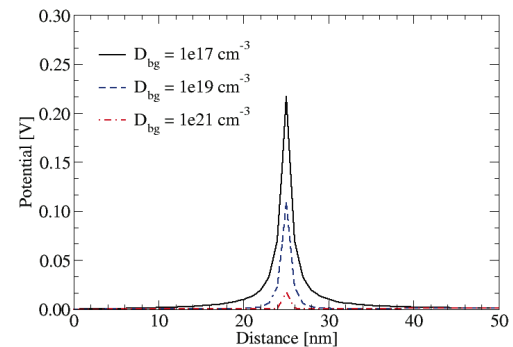


Figure 6. 1D electrostatic potential in the case of one discrete dopant at the center of the resistor with different continuous background doping densities.

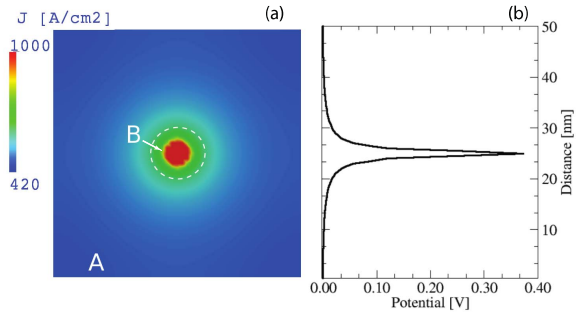


Figure 7. (a) Current density in the median plane between source and drain in the case of one discrete dopant placed at the center of the resistor, and (b) corresponding 1D electrostatic potential.

This current flow between dopant atoms becomes more important as the number of dopants in the device becomes small. For this reason the error curve of Fig.4 start to decrease towards low doping densities. Even though the error is reduced at low dopant numbers there is a secondary effect associated with the position of dopant atoms. Fig. 8(a) shows the normalized error in the resistance for different numbers of dopants extracted from the different doping densities. It can be seen that even if the dopant numbers are the same, at low numbers there is a spread in the error coming directly from the positional effect. This spread in error values is large at low doping densities and strongly decreases at high doping densities. Indeed, in the presence of percolative conduction the relative position of dopants has a strong impact in determining the resistance of atomistic devices. This is also evident in Fig. 8(b) where the slope of the normal probability plot of the resistance error increases with the number of discrete dopants. Moreover it should be noted that the error in the resistance (Fig. 4) tends to zero when the number of dopants is very small, regardless of whether DG or a classical approach is used. This again confirms that, in presence of very few dopants, the current mainly flows outside the sphere of influence of the potential wells.

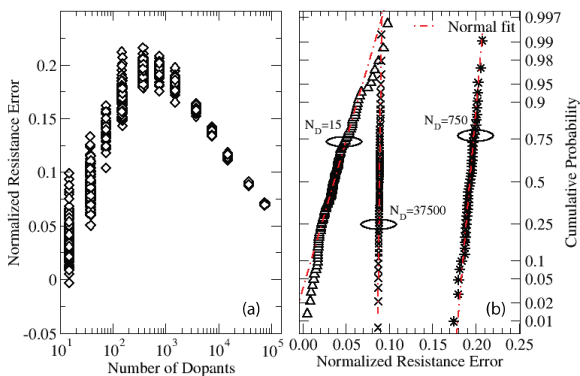


Figure 8. (a) Resistance error for each atomistic device for fixed values of number of dopants in the resistor, and (b) corresponding normal probability plot for three values of number of dopants.

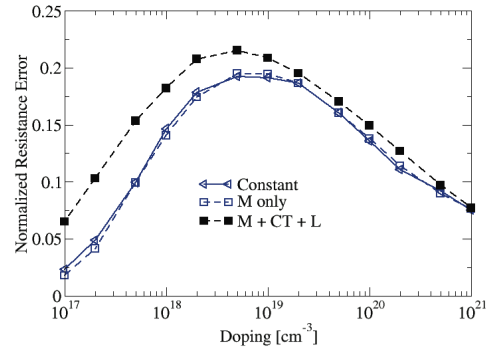


Figure 9. Resistance error curve for different mobility models: Constant, Masetti[6] (M), Caughey-Thomas[7] (CT) and Lombardi[8] (L).

The previous results have been obtained using only the Masetti[6] mobility model. If field dependent mobility models such as Caughey-Thomas[7] or Lombardi[8] are included we obtain the results shown in Fig. 9. Here it can be observed that there is an increase in the error due to the electrostatic potential wells associated with each discrete dopant in ‘atomistic’ simulations. However, this increase in the resistance error is negligible at high doping densities, due to the Debye screening, and remains small at low doping densities, due to the percolative regime.

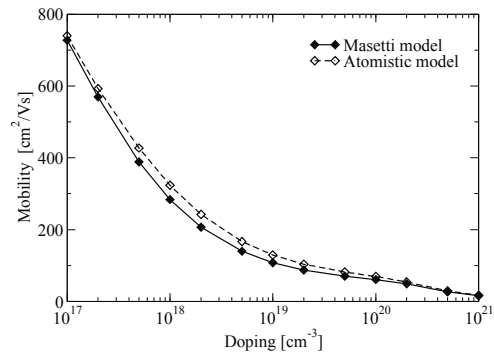


Figure 10. Electron mobility used to remove the resistance relative error (dashed line) compared to the Masetti model mobility (solid line) used for the continuously doped devices.

Parameter	Continuous	Atomistic
μ_0	1417	1429
μ_{min1}	52.2	52.2
μ_{min2}	52.2	52.2
μ_1	43.4	45
P_c	0.0	0.0
C_r	$9.68 \cdot 10^{16}$	$9.81 \cdot 10^{16}$
C_s	$3.43 \cdot 10^{20}$	$3.48 \cdot 10^{20}$
α	0.68	0.61
β	2	2

Table 1. Masetti model parameters values extracted to obtain a match, within 0.5% of error, between the continuously doped device resistance and the average ‘atomistic’ device resistance.

The previous analysis suggests that (i) in attempting to eliminate the error from the simulations the effects of the electric field can be ignored and (ii) the error in the resistance can be removed by modifying the mobility in ‘atomistic’ simulations according to:

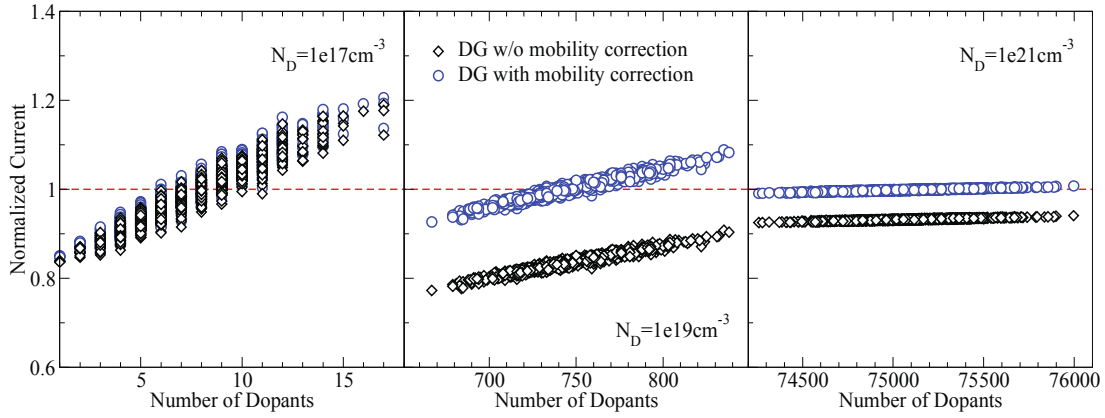


Figure 11. Scatter plot of ensembles of 1000 atomistically doped 50x50x50nm silicon resistors, with currents normalized to the analytical average case for doping densities of $1 \times 10^{17} \text{ cm}^{-3}$, $1 \times 10^{19} \text{ cm}^{-3}$ and $1 \times 10^{21} \text{ cm}^{-3}$.

$$\mu_{atomistic}(N_D) = [1 + err(N_D)] \cdot \mu_{continuous}(N_D)$$

where $\mu_{continuous}(N_D)$ is the mobility used in simulations of continuously doped resistors and $err(N_D)$ is the DG resistance error of Fig. 4. It is clear that $err(N_D)$ is defined only for a finite number of discrete values so an interpolation strategy is required, especially when this correction is applied to the simulation of MOSFETs with non-uniform doping profiles. A better strategy is to adopt an analytical expression for the corrected ‘atomistic’ mobility. In the rest of this paper we employ the second method.

Fig. 10 shows the electron mobility that should be adopted in the ‘atomistic’ simulations to match the resistance of the continuously doped devices, comparing it with the conventional Masetti model mobility [6]. It is important to note that the ‘atomistic’ mobility only slightly differs from the Masetti model. This suggest that an analytical expression for the ‘atomistic’ mobility model can be found by modifying the parameters of the Masetti model, without introducing any other complex relationship.

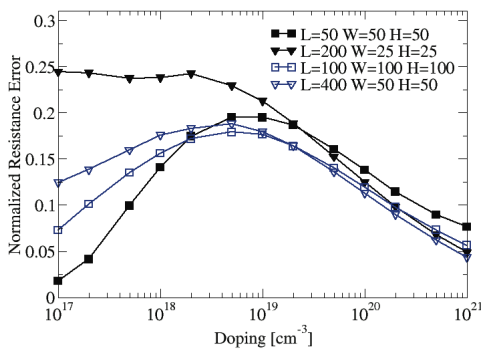


Figure 12. Resistance error curve for a 50x50x50nm (filled symbols) and a 100x100x100nm (open symbols) resistors with two different aspect ratio.

Table 1 reports the conventional and the modified values for the Masetti model parameters obtained to have an error in the resistance of less then 0.5% over the whole range of doping densities. Fig. 11 shows the scatter plot of ensembles of 1000 atomistically doped silicon resistors, with currents normalised to the continuously doped case for doping densities of 1×10^{17}

cm^{-3} , $1 \times 10^{19} \text{ cm}^{-3}$ and $1 \times 10^{21} \text{ cm}^{-3}$. It is evident that the mobility correction remove the resistance error without introducing distorsions in the original statistical distribution.

Finally, Fig. 12 points out that the percolative nature of the conduction at low doping densities makes the error dependent on the aspect ratio of the device. As expected, a shrinking in the resistor cross-section (maintaining a constant volume) results in an increased error at low doping. This effect becomes more prominent as the volume of the resistor is reduced. However it affects only the low doping region, that is usually irrilevant in the simulation of MOSFET source and drain regions. Moreover Fig. 12 shows that the error curve remains almost unchanged when increased to nearly ten times the volume of the resistor ($50 \times 50 \times 50 \text{ nm}^3$ to $100 \times 100 \times 100 \text{ nm}^3$). This confirms that the charge trapping is an artifact of ‘atomistic’ simulations and that the analytical resistance represents a good choice of reference with which to compute the resistance error.

IV. CONCLUSIONS

In conclusion, we presented a comprehensive 3D statistical study of the increase in resistance associated with charge trapping in ‘atomistic’ simulations, considering a wide range of doping densities and mesh spacing. A modified mobility model for the ‘atomistic’ simulations was proposed to suppress the error related to the fictitious charge-trapping. The results are of utmost importance for the correct ‘atomistic’ modeling of source/drain access resistance in scaled MOSFET devices.

Acknowledgments. The authors would like to thank A. S. Spinelli and C. Monzio Compagnoni from Politecnico di Milano for the useful discussions. This work was partially supported by the EU through the ENIAC-120003 MODERN program.

REFERENCES

- [1] A. Asenov, IEEE Trans. Electron Dev., 45, 2505 (1998).
- [2] T. Ezaki, et al., Proc. SISPAD, 91 (2002).
- [3] N. Sano et al., Microelec. Reliability, 42, 189 (2002).
- [4] G. Roy, A. R. Brown, A. Asenov and S. Roy, Journal of Computational Electronics, 2, 323 (2003).
- [5] R.W. Hockney and J.W. Eastwood, Computer Simulation Using Particles (IoP Publishing, Bristol, 1999).
- [6] G. Masetti, M. Severi, and S. Solmi, IEEE Trans. Electron Dev., 30, 764 (1983).
- [7] D. Caughey, R. Thomas, Proc. IEEE 55, 2192 (1967)
- [8] C. Lombardi, S. Manzini, A. Saporito, M. Vanzi, IEEE TCAD, 7, 1164 (1988).